

# Chirality Analysis for Nanostructured Microparticles Using Deep Learning

Anastasia Visheratina,<sup>a,†</sup> Alexander Visheratin,<sup>b,†</sup> Prashant Kumar,<sup>a</sup> Michael Veksler,<sup>a</sup>  
Nicholas A. Kotov<sup>a,\*</sup>

<sup>a</sup> *Biointerfaces Institute, University of Michigan, Ann Arbor, Michigan, USA*

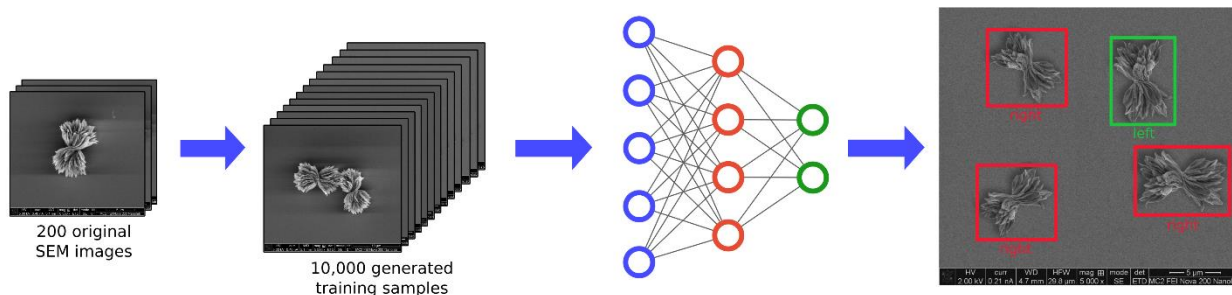
<sup>b</sup> *Beehive AI, San Francisco, California, USA*

**KEYWORDS:** biomimetic nanostructures, deep learning, image analysis, Siamese learning, chiral nanoparticles, scanning electron microscopy

\* To whom correspondence should be addressed:

Nicholas A. Kotov ([kotov@umich.edu](mailto:kotov@umich.edu))

† These authors contributed equally



Visual representation of the deep learning training process for the detection and classification of chiral nanostructured microparticles.

**ABSTRACT:** Chirality of helical objects, exemplified by nanostructured inorganic particles, has unifying importance for many scientific fields. Their handedness can be determined visually, but its identification by analysis of electron microscopy images is fundamentally difficult because (1) image features differentiating left- and right-handed particles can be ambiguous and ancillary, and (2) three-dimensional particle structure essential for chirality is 'flattened' into two-dimensional projections. Here we show that deep learning algorithms can reliably identify and classify twisted bowtie-shaped microparticles in scanning electron microscopy images with accuracy as high as 94.4% having been trained on as few as 180 images. Furthermore, after training on bowtie particles with complex nanostructured features, the model can recognize *other* chiral shapes with different geometries without re-training. These findings indicate that deep learning can potentially replicate the visual analysis of chiral objects by humans and enable automated analysis of microscopy data for accelerated discovery of chiral materials.

## Introduction

The unique optical, biological, and electrical properties of chiral nanostructured particles strongly depend on the helicity of their nano-, meso-, and microscale shapes.<sup>1-7</sup> Unlike similarly-sized chiral objects of (bio)organic origin, the shapes of chiral inorganic particles can be readily identified from electron microscopy (EM) images, which markedly streamlines the research process. However, the chiral nanostructures are polydispersed, necessitating simultaneous assessment of their chirality, size, shape, and variability.<sup>8,9</sup> Methods and tools for computational analysis of sizes and polydispersity are abundant, but the same is not true for chirality, which is fundamentally more difficult. Analysis of EM images for chirality is tedious and the 'manual' image processing is subject to experimentalist bias.

While visual recognition of helical objects by humans was developed over many years of evolution, the same task for machine vision is problematic and has not been solved so far. The first problem is that the image attributes differentiating left- and right-handed enantiomers in EM images are subtle and can be ambiguous. Other image features represented, for instance, by nanoscale structuring of the particles, often dominate the feature space. The second problem is that the vast majority of EM images are two-dimensional (2D) projections of three-dimensional (3D) objects, which results in a large amount of information specific to chirality being lost. 3D versions of EM techniques are rapidly developing, but the acquisition of such images is non-trivial and, in fact, impossible for many substances because of electron beam damage.<sup>10</sup> Furthermore, the long time required for 3D EM scans makes this method currently unsuitable for statistical evaluation of chiral shapes and calculation of their enantiomeric excess. 2D EM data are much more prevalent and, when obtained with sufficient quality and quantity, can potentially provide the required information.

Implementation of machine learning (ML) algorithms is transforming EM methods<sup>11,12</sup> enabling, for example, automated detection and analysis of size and shape distributions of nanoparticles from transmission electron microscopy (TEM),<sup>13,14</sup> scanning electron microscopy (SEM),<sup>15–17</sup> helium ion microscopy,<sup>18</sup> and scanning tunneling microscopy<sup>19</sup> images. However, chirality detection requires a more potent methodology of deep learning (DL) – a subfield of ML that employs neural networks to solve complex human-like image recognition problems. DL has been widely employed in computer vision<sup>20</sup> and is even more advantageous in EM by improving signal-to-noise ratio, aberration correction, and reducing specimen drift<sup>21–28</sup> thereby increasing the resolution of SEM,<sup>29–31</sup> STEM,<sup>32</sup> and TEM.<sup>33</sup> Other emerging applications of DL include image labelling for identifying different image regions<sup>34–38</sup> and semantic segmentation classifying pixels into discrete categories.<sup>39–42</sup> However, until now most ML and DL applications in EM have focused on nanoparticles that are shape-similar. Recognition of chirality in nanostructures using DL has not been realized yet. Detection and classification of chiral nanostructures from EM images screening multiple left/right nanoscale geometries will provide game-changing tools for the development of chiral nanostructures for photonics and other technologies.

Here, we developed DL models to detect a diverse spectrum of chiral nanostructures on SEM images and classify them based on their handedness. We used nanostructured particles with bowtie shapes because they can be synthesized with right-/left-handed twists as well as with different length, width, thickness, and twist angle. We applied DL algorithms to 2D SEM images where the twist in bowties can be easily recognized by the human eye and potentially be used to characterize their 3D chirality. Two DL algorithms were tested to overcome the intrinsic limitations of exceptionally large databases comprising thousands and millions of images previously required for successful models training. We show that a realistic database with as small as 180 SEM images is sufficient for achieving an accuracy of bowtie detection in SEM images as high as 94.4%. One of the algorithms was able to classify bowties on right-/left-handed with 79% accuracy. Furthermore, we tested our models on SEM images of chiral inorganic particles with different geometries that they had not 'seen' before. Without re-training, our models can detect novel chiral structures with an accuracy as high as 93%, indicating the biomimetic *learning* abilities of the employed neural networks. The developed algorithms can be further expanded to accommodate analysis of other parameters relevant for fundamental and technological applications of chiral nanostructures and be integrated with complementary microscopy and spectroscopy methods.

## **Results and Discussions**

### **1. Particle Chirality and Machine Learning**

Despite the ubiquity and importance of chiral structures around us, the nexus between chiral objects and machine learning (ML) is an unexplored territory. This work is intended to make inroads in this direction, specifically for microscopy images of chiral nanostructured microparticles, which can be subsequently extended both to chiral objects both at smaller and larger scales. The foundational hypothesis for this study is that trained deep learning (DL) algorithms will enable automatic identification of right- and left-handed versions of mirror asymmetric particles. As an experimental model, we used nanostructured right- or left-handed particles of bowtie shape because their DL-based recognition and classification can be verified by independent image processing, and these particles have strong polarization rotation, high surface area, and other technologically attractive properties. Furthermore, particles with shapes containing twisted elements can be made from a variety of materials,<sup>5,43–46</sup> and their length, width, thickness, and twist angle can vary widely for different materials.

Besides the 2D nature of the SEM images that makes identification of chirality fundamentally challenging, DL-based analysis of particle images also has additional challenges. *First*, typical DL-based approaches for computer vision require tens of thousands of images to properly train the model.<sup>47,48</sup> Although theoretically feasible, such large number of images is prohibitive for any EM technique, including SEM. *Second*, the handedness of the bowties is determined by their twist, which is mostly observed in the center of the nanostructured bowtie (**Figure 1a**). Closer to the periphery of the bowtie, the twist becomes less pronounced, being replaced with a rich spectrum of nanoscale features that are nearly identical for the left- and right-handed particles. This means that the relatively small area of the bowtie (**Figure 1a**, blue rectangle) is responsible for its classification. In some circumstances (e.g., bowties overlapping), this specific feature of chiral shapes can make it even more difficult to quantify. *Third*, the directionality of the twist in 3D space reconstructed by our brains is the main criterion of the visual assessment of handedness of helical objects. However, rotation of the bowties by 90° leads to chiral structures with seemingly opposite handedness in 2D (**Figure 1b**). The same is true for many other helicoids. Also, this effect can complicate training and testing datasets, especially when particles have a different aspect ratio fitting, for example, a square and rectangle, leading to erroneous classification of their handedness. To address these problems, we applied two approaches based on *Siamese learning* (**Section 2.1**) and synthetic data generation (**Section 2.2**).

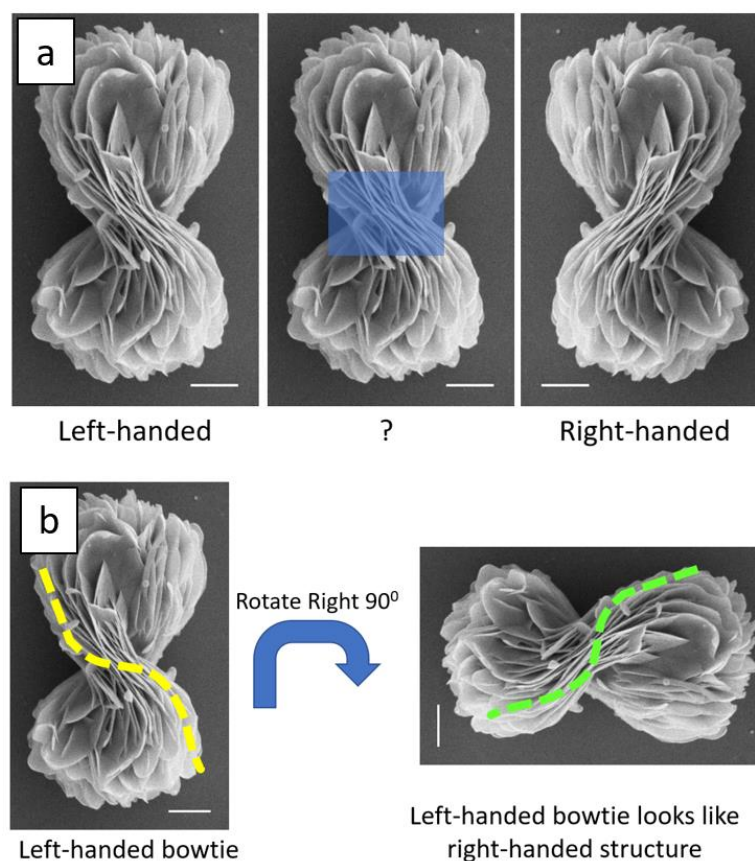


**Figure 1.** Challenges for the chirality determination of chiral nanostructured bowties associated with: (a) localization of the twisted area of bowties carrying the most information about their chirality (blue rectangle) (b) perception of bowtie chirality due to rotation of bowties by  $90^\circ$ , which leads to chiral structures of seemingly opposite handedness in 2D images. Scale bars:  $1\ \mu\text{m}$ .

## 2. Methods for Chirality Recognition by Deep Learning

### 2.1 Siamese learning

Artificial neural networks (ANNs) utilizing *Siamese learning* algorithms are widely used for image recognition,<sup>49</sup> natural language processing,<sup>50</sup> drug development,<sup>51</sup> medicine,<sup>52</sup> and theoretical physics.<sup>53</sup> ANNs with Siamese learning generally are class-agnostic<sup>51,54</sup> meaning that a trained ANN can theoretically identify a variety of objects with similar key feature(s), which is particularly suitable for chirality.

Furthermore, *Siamese learning* algorithms can be trained with minimal supervision – data labeling – that can be exceptionally time-consuming. Relaxing the supervision requirements is achieved by using combinations of target elements (images, texts, etc.) – pairs<sup>55</sup> or triplets,<sup>56</sup> depending on the optimization function used – for training. For example, if there are two classes in the dataset, each having 100 samples, it is possible to create 10,000 pairs by combining every sample from one class with every sample of another class.

In case of nanostructured microparticles with bowtie shapes, we use triplets: groups of three images (**Figure 2**), one of which is the anchor, another is from the same class as the anchor (positive), and the third is from a different class (negative). Then, the two classes are the images that contain bowties and images that do not. Each image from the triplet is passed through the ANN that converts it to feature vectors – a one-dimensional array of floating-point numbers. As a result, for every triplet, we get three feature vectors. We calculate after that the value of the optimization function – triplet loss.<sup>57</sup> This function determines whether (1) images from different classes are far enough in the feature space (and thus can be recognized) and (2) images from the same class are close (and thus can be classified). The better the calculated feature vectors satisfy these conditions, the smaller the value of the triplet loss. The aim of the network training is to ensure that feature vectors will be similar for images of the same class (e.g., bowties) and very different for images of different classes.

Unlike the previously used methods of Siamese learning by neural networks,<sup>58</sup> we used one network that generated feature vectors for all inputs instead of using two identical branches with shared weights that are combined into the distance metric. We experimentally acquired 180 SEM images, served as inputs for the neural network training. Of them, 90 images contained bowties and 90 did not. From these experimental images, we generated 11,888 triplets and split them into training and validation sets of 10,112 and 1,776 triplets, respectively. We applied random transformations (e.g., vertical and horizontal flips, rotation, brightness, and sharpness changes) to input images during training to prevent the neural network from overfitting.<sup>59</sup>

As a target neural network for feature vectors generation, we used *EfficientNet*<sup>60</sup> Python module since it is one of the state-of-the-art models for image processing because it provides the best combination of quality and training speed based on our data with bowtie particles (**Section S1** of Supporting Information). We used the *EfficientNet B4* without a classification head, so the model outputs a vector of size 1,792. We added two linear layers connected via the *GELU* activation function<sup>61</sup> to reduce the feature space size. As a result, the final model produces a vector of size 256. During the experimental evaluation, we tried the model that generates vectors of size 512, but it provided considerably worse performance due to the larger feature space.

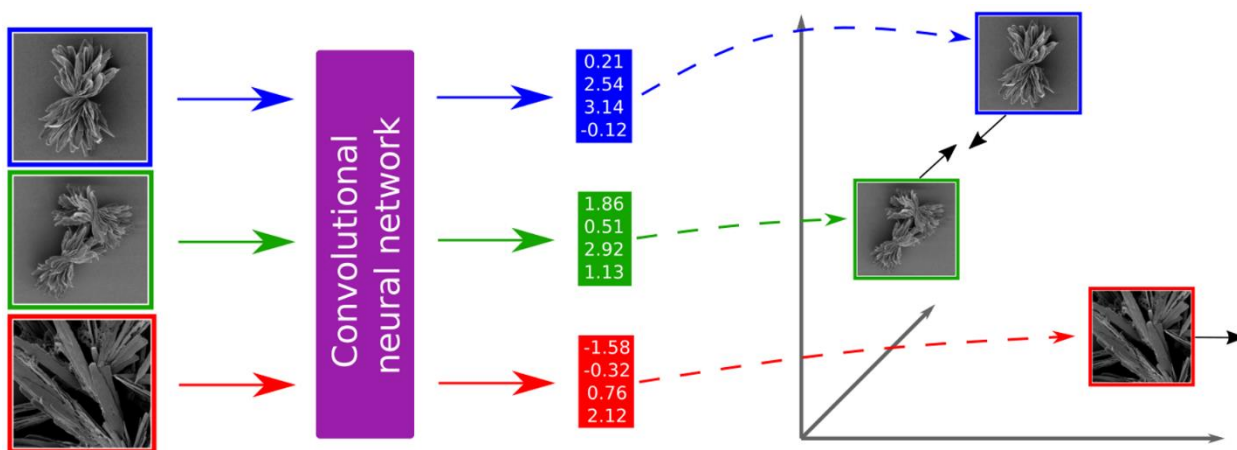


**Figure 2.** Siamese learning protocol for chiral microparticles. Anchor (blue), positive (green), and negative (red) images are passed through the ANN that outputs corresponding vectors of length  $N$ . The vector represents the position of the image in the  $N$ -dimensional embedding space. The closer the images are in the embedding space, the more similar they are from the ANN point of view. The goal of training is to bring images of the same class close to each other while keeping images of different classes far apart.

We trained the algorithm for six epochs using a batch size of 16, the Adam optimizer<sup>62</sup> and one cycle learning rate scheduler<sup>63</sup> for improved model convergence. The combination of minimum learning rate of  $1e^{-4}$  and maximum learning rate of  $1e^{-3}$  demonstrated the best results during hyperparameter tuning. For the triplet loss, the margin of 50 showed the best performance overall – lower values did not produce enough distinction between classes in the feature space; for higher values, the model struggled to distribute samples in the feature space properly.

To test the performance of the final model, we generated feature vectors for the training data and created a nearest centroid classifier<sup>64</sup> using them. After that, we applied the classifier to the test samples – 18 images (nine with bowties, nine without) that were not used in training. Precision as high as 94.4% was obtained with the distribution of train and test samples in the search space (**Figure S1**). We applied the t-SNE algorithm<sup>65</sup> to reduce the number of dimensions from 256 to 2 and plot the feature vectors. We can see that samples form two distinct groups and all test samples except for one correctly fit into their respective groups.

Bowtie detection is first in chirality analysis, with handedness determination coming second. To better understand the perception of SEM images by ANN, saliency maps of backpropagation gradients were analyzed after passing images through the model (**Figure 3**). These maps show which input image pixels contribute the most to the model's output and are widely used for the performance assessment of convolutional neural networks.<sup>66,67</sup> We can see that the network successfully distinguished pixels of bowties (**Figure 3a, Figure 3b**) and other parts of the image without the chiral object of interest (**Figure 3c**). These saliency maps confirmed the correctness of the model training, but they also demonstrated the challenge that the ANN faces. When trying

to identify left- and right-handed bowties, ANN has to locate small areas of difference (**Figure 1a**) without knowing where they are during training. Additionally, there can be bowties of different handedness in the same image, which would make it quite difficult for the neural network to classify the chiral objects.

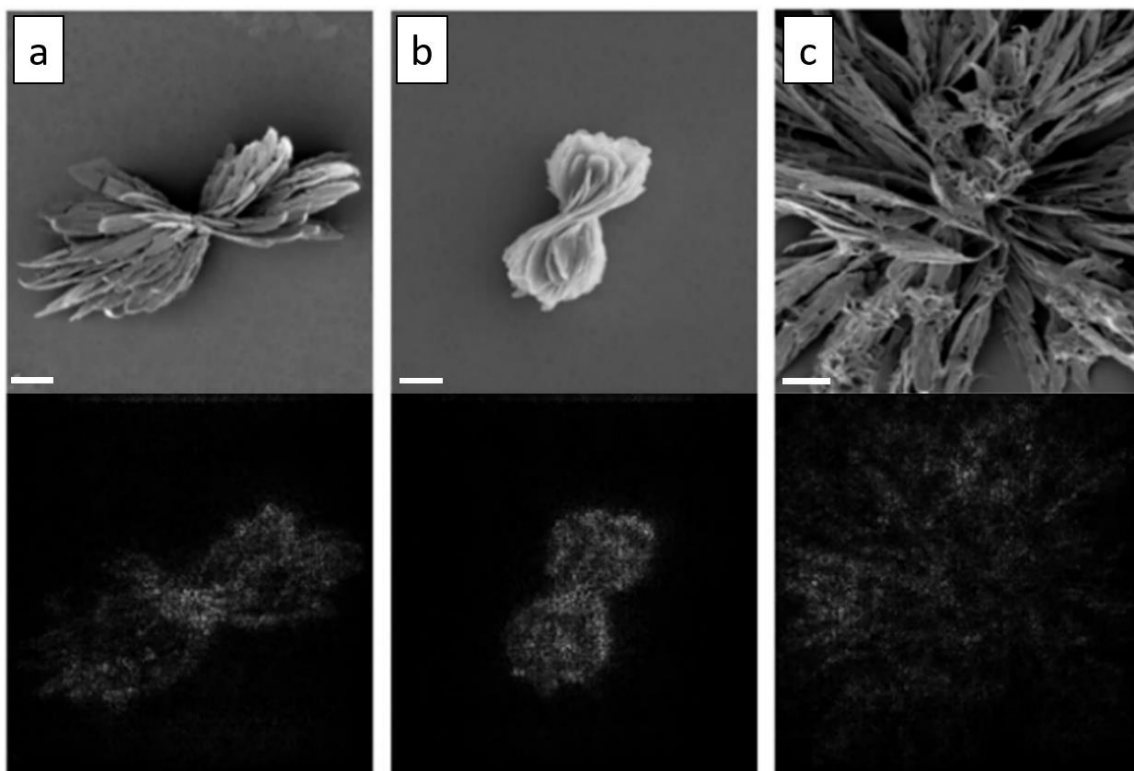


**Figure 3.** SEM images (top) and corresponding saliency maps (bottom) for a sample triplet: (a) anchor, (b) positive, (c) negative. Scale bars: 1  $\mu\text{m}$ .

## 2.2. Generation of synthetic SEM images

To identify the handedness of the bowties, we developed the second DL model based on creating a synthetic dataset from a small set of real images. This approach is used for a variety of applications,<sup>68–70</sup> and, according to *MIT Technology Review*, is one of ten Breakthrough Technologies 2022.<sup>71</sup> With respect to analysis of SEM images,<sup>16,72</sup> the methodology of synthetic datasets is not only novel but also powerful because it addresses one of the key problems – the limited amount and high cost of original data.

The first step in this algorithm is to create the database consisting of (1) background images without any particles and (2) particles images cut out from the background (**Figure 4**). From every SEM image, the algorithm precisely cuts particles (**Figure 4b**) and fills the image with substrate patches, so it looks like no particles were present (**Figure 4b**, bottom). The images of extracted particles are mirrored to obtain representations of both right- and left-handed objects (**Figure 4b**, top). Compared to *Siamese learning*, this method can be considered as supervised. However, once

the object database is created, the chirality and location of bowties are already known, so there is no need to do it manually. Also, depending on the number of objects extracted and their transformation, it is possible to generate any number of images. We note, however, that this method is the best for objects that can be extracted from the microscopy images. Its applicability to other chiral nanostructured and biological materials, such as fibrils, nets, can be limited, but it can be successfully overcome by *Siamese learning*.

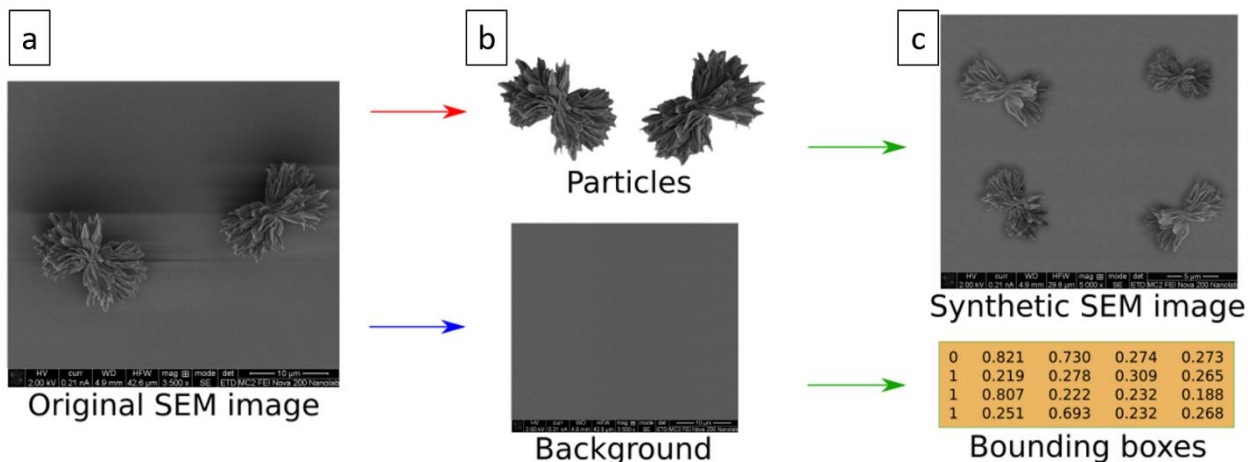


**Figure 4.** Generation of synthetic datasets from SEM images for ANN training: (a) example of original SEM image of bowties, (b) extracted bowties and backgrounds, and (c) example of generated SEM image and bounding box with information about particles in the image.

The second step is the generation of synthetic EM images (Supporting Information, **Section S2**), which provides the control over the number of particles in the image and their positions, sizes, and handedness. The algorithm outputs the information about particles in the image along with the image itself (**Figure 4c**). The first number is the class of the bowtie (0 is right-handed, 1 is left-handed), the following two numbers are relative positions of the center of the particle bounding box, and the last two numbers are relative sizes of the particle bounding box. This is the format required for the specific model that is commonly used in experiments. Depending on the task at hand, the format and properties extracted (e.g., width, height) can be different.

The third step is the training of the neural network. We used the *YOLOv5*<sup>73</sup> – a state-of-the-art algorithm capable of finding objects in images and classifying them. This algorithm is also known for its fast execution speed, making it a perfect candidate for embedded imaging systems like microscopes. *YOLOv5s* variant was implemented in this work because it is the fastest from this family of DL models (Supporting Information, **Section S3**). For our experiments, 10,200 images were generated for the training dataset and 1,500 images for the validation dataset. The

model reached a 99% f1 score and 99% mean average precision, which means that the model successfully learned how to determine chiral particles.

To test the algorithm performance on real data, we ran the detection on 195 original SEM images of bowtie particles that did *not* use during the training (**Figure 5**). Nevertheless, the DL algorithm can detect and classify bowties of different sizes, orientations, and aspect ratios, which can then allow it to automatically calculate the enantiomeric excess and other parameters of corresponding samples. The model yielded 91% precision for identifying the chiral particles and 79% precision for identifying their handedness.

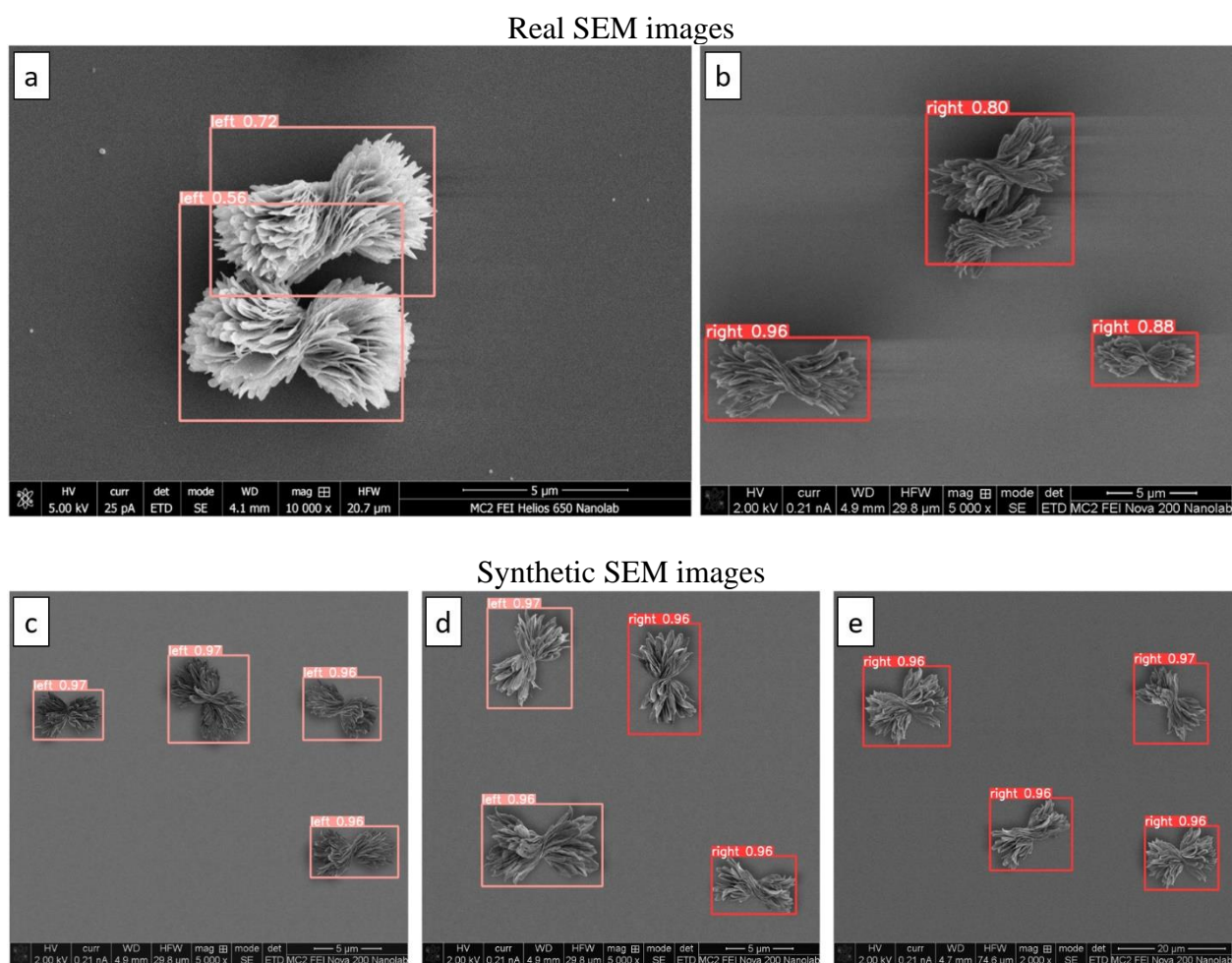


**Figure 5.** Examples of classification of bowties on right-handed and left-handed using real (a, b) and synthetic (b-e) SEM images.

### 3. Detection and classification of new chiral objects

To test the neural networks described in **Section 2**, we prepared datasets of geometrically different chiral and achiral structures that neural networks have not 'seen' before. Here, we want to understand the potential of developed models trained on particular chiral structures for the detection and classification of new chiral particles with potentially different shapes. The novel

structures included chiral Au-S 'twisted bundle' particles,<sup>1</sup> achiral Au-S 'kayak' particles,<sup>1</sup> and achiral 'pancake stack' particles made similar to bowties but using amino acid racemate<sup>74</sup>. The classifier based on the *Siamese learning* model detected these chiral objects previously unseen by the neural network with 82.5% accuracy, indicating that employed neural networks *learned* the concepts of chiral particles which are hierarchically organized. The t-SNE plot presented in **Figure S3** shows that most novel structures are distributed across bowties. We believe that the distinct shape of such hierarchically organized particles is one of the most critical factors for the model to detect and classify them. Therefore, achiral 'pancake stack' structures, which have a very clear shape in SEM images, were classified closer to the bowties.

The *YOLOv5* model was also able to differentiate between chiral and achiral Au-S structures with 93% accuracy. Simultaneously, it did not recognize 'pancake stack' particles as a chiral structure, which is equally important. Thus, twist is likely to be the key element enabling the recognition of chiral particles, which is quite similar to human perception of the 3D chiral geometries (**Figure 6**). The DL algorithm was able to classify Au-S structures on left and right with 64% accuracy, which is quite remarkable considering that these particles had a different morphology than bowties and the model was *not* trained on these particles. Further training can certainly increase this accuracy to the values similar to bowties, but at this point, it was important that the model was able to recognize left- and right chirality as a common feature in different types of particles without specific training on particles with different chiral shapes.

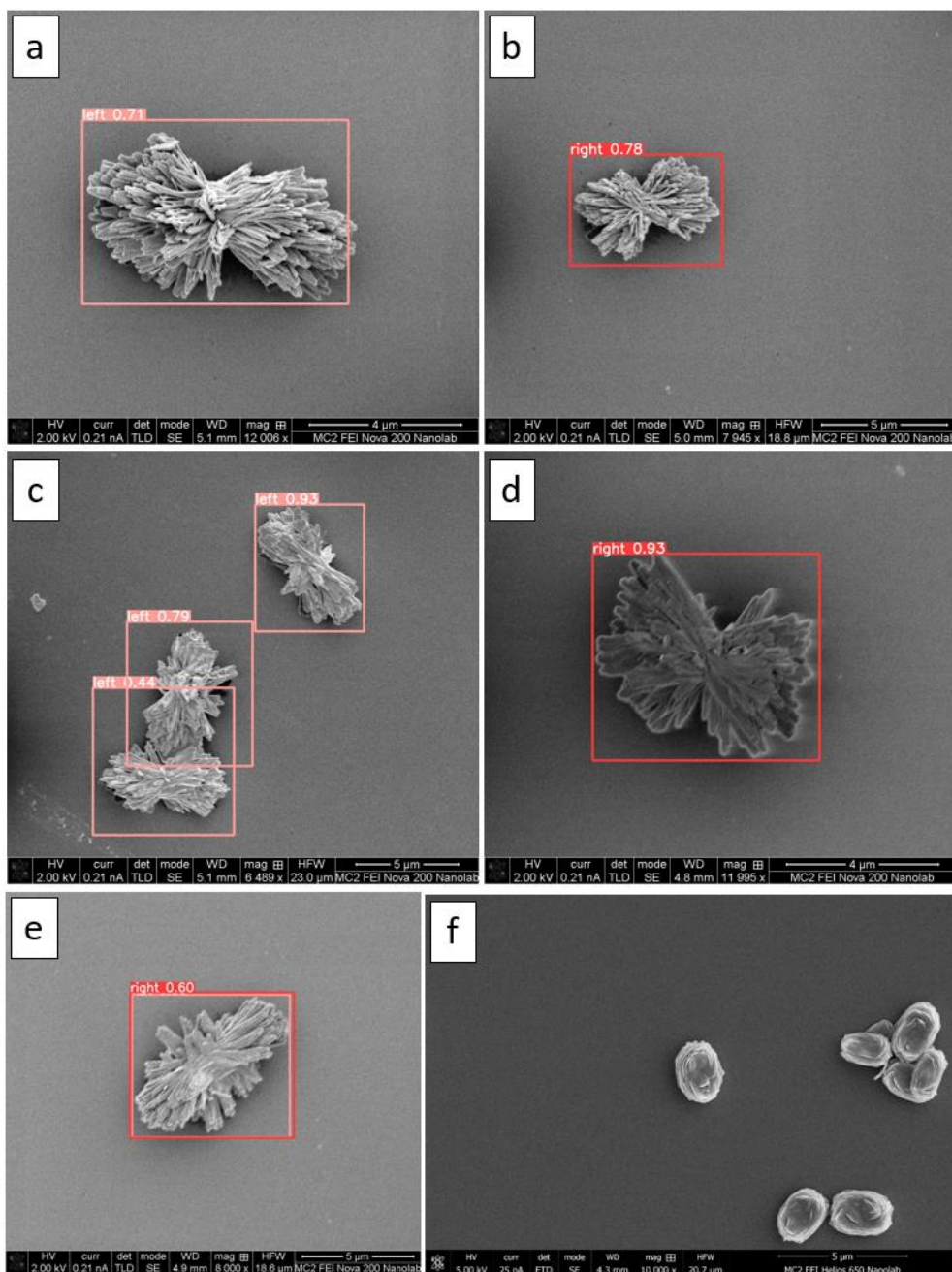


**Figure 6.** Examples of classification of chiral Au-S particles on left-handed (a, c) and right-handed (b, d) in SEM images. Detection of achiral structures in SEM images: achiral 'kayak' particles (e) and achiral 'pancake stack' structures (f).

## Conclusions

Chiral nanostructured microparticles offer solutions for biomedicine, optoelectronics, and photonics due to their outstanding optical properties, high chiroptical activity, and enantioselective interaction with biological objects.<sup>75</sup> DL-based analysis of electron microscopy images of chiral inorganic particles allows for the establishment of their chiral configuration, which will not only dramatically hasten their characterization but provide a powerful methodology for the accelerated

discovery of chiral nanostructures for a variety of materials needs. DL-based algorithms that can find chiral nanostructured microparticles of bowtie shape in SEM images and classify them as right- or left-handed depending on their chirality. Our results and the high processing speed (20 - 30 ms per image) open a realistic perspective of the practical application of these methods for automatic real-time analysis of electron microscopy images at scale, which can greatly simplify their property optimization and technological translation.

Methods described in the paper help overcome the need for collecting large datasets of microscopy images by using image triplets (**Section 2.1**) or synthetic images (**Section 2.2**) in algorithm training. Nevertheless, the increase of dataset size is likely to further increase accuracy of the DL classifications and should be pursued for their further development. For Siamese learning, the number of potential triplets scales non-linearly – going from 2 to 4 classes with 100 images in each will increase the number of triplet combinations six times. For synthetic image generation, the increase in the potential number of training samples increases even more because there is no hard limit in the number of images that can be generated from one dataset. We will need to further develop strategies for training datasets creation such that they (1) preserve reasonable training time and (2) ensure that the training dataset is diverse enough to keep the models generalizable.

The second problem to be aware of is the complexity of data. When we add more and more particle types to the training dataset, it may become increasingly challenging for the models to distinguish them. At some point, the base models that we used in this paper (*EfficientNet B4* and *YOLOv5s*) may need to be replaced with even more sophisticated ANNs. The larger and more complex versions – *EfficientNet B5-B7* and *YOLOv5m-x* will be tested to accommodate a greater variety of chiral scales and nanoscale features. We perform scaling down the embedding vector to 256. Moreover, in *Siamese learning*. In addition to the use of these networks, it is possible to increase the size of the resulting vector (512, 1024, or original size) to create a larger embedding space that can fit more particle types. Described changes will further increase the training time but create room for automated analysis of a wide variety of microscopy images.

We also expect that it is hard to visually determine object properties (size, chirality) or even separate different objects themselves, which is typical for complex images containing nanofibrils, nanoclusters, or dendritic nanostructures. A comprehensive database for synthetic images generation will be more difficult to create for such raw data.

In perspective, further development of DL for chirality can be used to predict microparticle properties based on their chiral shapes and nanoscale morphology that would be complementary to electromagnetic and quantum mechanical calculations.

## Materials and Methods

### *SEM data*

Structures of bowtie shape and 'pancake stack' shape were synthesized in an approach similar to that described in Ref.<sup>74</sup> with some modifications. Au-S structures were synthesized in an approach similar to Ref.<sup>1</sup> An FEI Nova 200 Nanolab Dual Beam SEM was used for SEM imaging.

### *Deep learning models training*

Both models used in this research were developed using the PyTorch (<https://pytorch.org/>) framework of version 1.10 with GPU support. We performed the training in the Google Colab environment (<https://colab.research.google.com/>) on NVIDIA P100 and V100 GPU accelerators.

Regarding the *YOLOv5s* training process, we followed official guidelines and used scripts provided by the library developers [<https://github.com/ultralytics/yolov5/wiki/Train-Custom-Data>]. The batch size was set to 32, resized image size (used to preserve uniformity of the input images) was set to 800 pixels, and the number of epochs was 2000.

## ASSOCIATED CONTENT

**Supporting Information.** Details on the Siamese network tuning, generation of synthetic SEM images, and optimization of YOLOv5 model.

## AUTHOR INFORMATION

### **Corresponding Author**

\*E-mail: Nicholas A. Kotov ([kotov@umich.edu](mailto:kotov@umich.edu))

### **Author Contributions**

The manuscript was written through contributions of all authors. All authors have given approval to the final version of the manuscript. A.V. and A.V. developed approaches for the chiral structures detection and classification and associated DL algorithms. P.K. carried out synthesis of bowties and 'pancake stack'-shaped structures and performed their SEM characterization. M.V. carried out synthesis of chiral and achiral Au-S structures and performed their SEM characterization. N.A.K. conceptualized and supervised the project. A.V., A.V. and N.A.K. analyzed the data and co-wrote the paper. † These authors contributed equally.

## Notes

The authors declare no competing financial interest.

## ACKNOWLEDGMENTS

The central part of this work was supported by the Vannevar Bush DoD Fellowship to N.A.K. titled "Engineered Chiral Ceramics" ONR N000141812876 and NSF project NSF 1566460 "Nanospiked Particles for Photocatalysis", NSF 1538180 is also gratefully acknowledged. Michigan Center for Materials Characterization (MC)<sup>2</sup> is acknowledged for its assistance with electron microscopy, and for the NSF grant #DMR-9871177 for funding of the JEOL 2010F analytical electron microscope used in this work. This work was also supported in part by the Office of Naval Research, MURI N00014-20-1-2479.

## References

- (1) Jiang, W.; Qu, Z.; Kumar, P.; Vecchio, D.; Wang, Y.; Ma, Y.; Bahng, J. H.; Bernardino, K.; Gomes, W. R.; Colombari, F. M.; Lozada-Blanco, A.; Veksler, M.; Marino, E.; Simon, A.; Murray, C.; Muniz, S. R.; Moura, A. F. de; Kotov, N. A. Emergence of Complexity in Hierarchically Organized Chiral Particles. *Science* (80-. ). **2020**, *368* (6491), 642–648. <https://doi.org/DOI: 10.1126/science.aaz7949>.
- (2) Smeets, P. J. M.; Cho, K. R.; Kempen, R. G. E.; Sommerdijk, N. A. J. M.; De Yoreo, J. J. Calcium Carbonate Nucleation Driven by Ion Binding in a Biomimetic Matrix Revealed by in Situ Electron Microscopy. *Nat. Mater.* **2015**, *14* (4), 394–399. <https://doi.org/10.1038/nmat4193>.
- (3) González-Rubio, G.; Mosquera, J.; Kumar, V.; Pedraza-Tardajos, A.; Llombart, P.; Solís, D. M.; Lobato, I.; Noya, E. G.; Guerrero-Martínez, A.; Taboada, J. M.; Obelleiro, F.; MacDowell, L. G.; Bals, S.; Liz-Marzán, L. M. Micelle-Directed Chiral Seeded Growth on Anisotropic Gold Nanocrystals. *Science* (80-. ). **2020**, *368* (6498), 1472 LP – 1477. <https://doi.org/10.1126/science.aba0980>.
- (4) Lee, H.; Ahn, H.-Y.; Mun, J.; Lee, Y. Y.; Kim, M.; Cho, N. H.; Chang, K.; Kim, W. S.; Rho, J.; Nam, K. tae. Amino-Acid- and Peptide-Directed Synthesis of Chiral Plasmonic Gold Nanoparticles. *Nature* **2018**, *556* (7701), 360.
- (5) Liu, H.; Shen, X.; Wang, Z.-G.; Kuzyk, A.; Ding, B. Helical Nanostructures Based on DNA Self-Assembly. *Nanoscale* **2014**, *6* (16), 9331–9338. <https://doi.org/10.1039/c3nr06913c>.

- (6) Park, K. H.; Kwon, J.; Jeong, U.; Kim, J. Y.; Kotov, N. A.; Yeom, J. Broad Chiroptical Activity from Ultraviolet to Short-Wave Infrared by Chirality Transfer from Molecular to Micrometer Scale. *ACS Nano* **2021**, *15* (9), 15229–15237.  
<https://doi.org/10.1021/acsnano.1c05888>.
- (7) Valev, V. K.; Baumberg, J. J.; Sibilia, C.; Verbiest, T. Chirality and Chiroptical Effects in Plasmonic Nanostructures: Fundamentals, Recent Progress, and Outlook. *Adv. Mater.* **2013**, *25* (18), 2517–2534. <https://doi.org/10.1002/adma.201205178>.
- (8) Ma, W.; Xu, L.; Moura, A. F. De; Wu, X.; Kuang, H.; Xu, C.; Kotov, N. A. Chiral Inorganic Nanostructures. *Chem. Rev.* **2017**, *117* (12), 8041–8093.  
<https://doi.org/10.1021/acs.chemrev.6b00755>.
- (9) Baimuratov, A. S.; Rukhlenko, I. D.; Noskov, R. E.; Ginzburg, P.; Gun'ko, Y. K.; Baranov, A. V.; Fedorov, A. V. Giant Optical Activity of Quantum Dots, Rods, and Disks with Screw Dislocations. *Sci. Rep.* **2015**, *5*, 14712. <https://doi.org/10.1038/srep14712>.
- (10) Ercius, P.; Alaidi, O.; Rames, M. J.; Ren, G. Electron Tomography: A Three-Dimensional Analytic Tool for Hard and Soft Materials Research. *Adv. Mater.* **2015**, *27* (38), 5638–5663.
- (11) Ede, J. M. Deep Learning in Electron Microscopy. *Mach. Learn. Sci. Technol.* **2021**, *2* (1), 11004.
- (12) Groschner, C.; Choi, C.; Nguyen, D.; Ophus, C.; Scott, M. Machine Learning for High Throughput HRTEM Analysis. *Microsc. Microanal.* **2019**, *25* (S2), 150–151.
- (13) Wen, H.; Luna-Romera, J. M.; Riquelme, J. C.; Dwyer, C.; Chang, S. L. Y. Statistically Representative Metrology of Nanoparticles via Unsupervised Machine Learning of TEM Images. *Nanomaterials* **2021**, *11* (10), 2706.
- (14) Lee, B.; Yoon, S.; Lee, J. W.; Kim, Y.; Chang, J.; Yun, J.; Ro, J. C.; Lee, J.-S.; Lee, J. H. Statistical Characterization of the Morphologies of Nanoparticles through Machine Learning Based Electron Microscopy Image Analysis. *ACS Nano* **2020**, *14* (12), 17125–17133.
- (15) Kim, H.; Han, J.; Han, T. Y.-J. Machine Vision-Driven Automatic Recognition of Particle Size and Morphology in SEM Images. *Nanoscale* **2020**, *12* (37), 19461–19469.
- (16) Kharin, A. Y. Deep Learning for Scanning Electron Microscopy: Synthetic Data for the Nanoparticles Detection. *Ultramicroscopy* **2020**, *219*, 113125.

- (17) Cid-Mejías, A.; Alonso-Calvo, R.; Gavilán, H.; Crespo, J.; Maojo, V. A Deep Learning Approach Using Synthetic Images for Segmenting and Estimating 3D Orientation of Nanoparticles in EM Images. *Comput. Methods Programs Biomed.* **2021**, *202*, 105958.
- (18) Mill, L.; Wolff, D.; Gerrits, N.; Philipp, P.; Kling, L.; Vollnhals, F.; Ignatenko, A.; Jaremenko, C.; Huang, Y.; De Castro, O.; others. Synthetic Image Rendering Solves Annotation Problem in Deep Learning Nanoparticle Segmentation. *Small Methods* **2021**, *5* (7), 2100223.
- (19) Okunev, A. G.; Mashukov, M. Y.; Nartova, A. V.; Matveev, A. V. Nanoparticle Recognition on Scanning Probe Microscopy Images Using Computer Vision and Deep Learning. *Nanomaterials* **2020**, *10* (7), 1285.
- (20) Madsen, J.; Liu, P.; Kling, J.; Wagner, J. B.; Hansen, T. W.; Winther, O.; Schiøtz, J. A Deep Learning Approach to Identify Local Structures in Atomic-Resolution Transmission Electron Microscopy Images. *Adv. Theory Simulations* **2018**, *1* (8), 1800037.
- (21) Ede, J. M.; Beanland, R. Improving Electron Micrograph Signal-to-Noise with an Atrous Convolutional Encoder-Decoder. *Ultramicroscopy* **2019**, *202*, 18–25.
- (22) Giannatou, E.; Papavieros, G.; Constantoudis, V.; Papageorgiou, H.; Gogolides, E. Deep Learning Denoising of SEM Images towards Noise-Reduced LER Measurements. *Microelectron. Eng.* **2019**, *216*, 111051.
- (23) Chaudhary, N.; Savari, S. A.; Yeddulapalli, S. S. Line Roughness Estimation and Poisson Denoising in Scanning Electron Microscope Images Using Deep Learning. *J. Micro/Nanolithography, MEMS, MOEMS* **2019**, *18* (2), 24001.
- (24) Vasudevan, R. K.; Jesse, S. Deep Learning as a Tool for Image Denoising and Drift Correction. *Microsc. Microanal.* **2019**, *25* (S2), 190–191.
- (25) Wang, F.; Henninen, T. R.; Keller, D.; Erni, R. Noise2Atom: Unsupervised Denoising for Scanning Transmission Electron Microscopy Images. *Appl. Microsc.* **2020**, *50* (1), 1–9.
- (26) Bepler, T.; Kelley, K.; Noble, A. J.; Berger, B. Topaz-Denoise: General Deep Denoising Models for CryoEM and CryoET. *Nat. Commun.* **2020**, *11* (1), 1–12.
- (27) Tegunov, D.; Cramer, P. Real-Time Cryo-Electron Microscopy Data Preprocessing with Warp. *Nat. Methods* **2019**, *16* (11), 1146–1152.
- (28) Vincent, J. L.; Manzorro, R.; Mohan, S.; Tang, B.; Sheth, D. Y.; Simoncelli, E. P.; Matteson, D. S.; Fernandez-Granda, C.; Crozier, P. A. Developing and Evaluating Deep

- Neural Network-Based Denoising for Nanoparticle TEM Images with Ultra-Low Signal-to-Noise. *arXiv Prepr. arXiv2101.07770* **2021**.
- (29) Fang, L.; Monroe, F.; Novak, S. W.; Kirk, L.; Schiavon, C. R.; Seungyoon, B. Y.; Zhang, T.; Wu, M.; Kastner, K.; Latif, A. A.; others. Deep Learning-Based Point-Scanning Super-Resolution Imaging. *Nat. Methods* **2021**, *18* (4), 406–416.
- (30) de Haan, K.; Ballard, Z. S.; Rivenson, Y.; Wu, Y.; Ozcan, A. Resolution Enhancement in Scanning Electron Microscopy Using Deep Learning. *Sci. Rep.* **2019**, *9* (1), 1–7.
- (31) Gao, Z.; Ma, W.; Huang, S.; Hua, P.; Lan, C.; others. Deep Learning for Super-Resolution in a Field Emission Scanning Electron Microscope. *AI* **2020**, *1* (1), 1–10.
- (32) Ede, J. M.; Beanland, R. Adaptive Learning Rate Clipping Stabilizes Learning. *Mach. Learn. Sci. Technol.* **2020**, *1* (1), 15011.
- (33) Suveer, A.; Gupta, A.; Kylberg, G.; Sintorn, I.-M. Super-Resolution Reconstruction of Transmission Electron Microscopy Images Using Deep Learning. In *2019 IEEE 16th International Symposium on Biomedical Imaging (ISBI 2019)*; 2019; pp 548–551.
- (34) Yokoyama, Y.; Terada, T.; Shimizu, K.; Nishikawa, K.; Kozai, D.; Shimada, A.; Mizoguchi, A.; Fujiyoshi, Y.; Tani, K. Development of a Deep Learning-Based Method to Identify “Good” Regions of a Cryo-Electron Microscopy Grid. *Biophys. Rev.* **2020**, *12* (2), 349–354.
- (35) Sanchez-Garcia, R.; Segura, J.; Maluenda, D.; Sorzano, C. O. S.; Carazo, J. M. MicrographCleaner: A Python Package for Cryo-EM Micrograph Cleaning Using Deep Learning. *J. Struct. Biol.* **2020**, *210* (3), 107498.
- (36) Aguiar, J. A.; Gong, M. L.; Unocic, R. R.; Tasdizen, T.; Miller, B. D. Decoding Crystallography from High-Resolution Electron Imaging and Diffraction Datasets with Deep Learning. *Sci. Adv.* **2019**, *5* (10), eaaw1949.
- (37) Vasudevan, R. K.; Laanait, N.; Ferragut, E. M.; Wang, K.; Geohegan, D. B.; Xiao, K.; Ziatdinov, M.; Jesse, S.; Dyck, O.; Kalinin, S. V. Mapping Mesoscopic Phase Evolution during E-Beam Induced Transformations via Deep Learning of Atomically Resolved Images. *npj Comput. Mater.* **2018**, *4* (1), 1–9.
- (38) Avramov, T. K.; Vyeniello, D.; Gomez-Blanco, J.; Adinarayanan, S.; Vargas, J.; Si, D. Deep Learning for Validating and Estimating Resolution of Cryo-Electron Microscopy Density Maps. *Molecules* **2019**, *24* (6), 1181.

- (39) Yi, J.; Yuan, Z.; Peng, J. Adversarial-Prediction Guided Multi-Task Adaptation for Semantic Segmentation of Electron Microscopy Images. In *2020 IEEE 17th International Symposium on Biomedical Imaging (ISBI)*; 2020; pp 1205–1208.
- (40) Fakhry, A.; Zeng, T.; Ji, S. Residual Deconvolutional Networks for Brain Electron Microscopy Image Segmentation. *IEEE Trans. Med. Imaging* **2016**, *36* (2), 447–456.
- (41) Roberts, G.; Haile, S. Y.; Sainju, R.; Edwards, D. J.; Hutchinson, B.; Zhu, Y. Deep Learning for Semantic Segmentation of Defects in Advanced STEM Images of Steels. *Sci. Rep.* **2019**, *9* (1), 1–12.
- (42) Ibtehaz, N.; Rahman, M. S. MultiResUNet: Rethinking the U-Net Architecture for Multimodal Biomedical Image Segmentation. *Neural Networks* **2020**, *121*, 74–87.
- (43) Ren, Z.; Gao, P.-X. A Review of Helical Nanostructures: Growth Theories, Synthesis Strategies and Properties. *Nanoscale* **2014**, *6* (16), 9366–9400.
- (44) Haddad, A.; Aharoni, H.; Sharon, E.; Shtukenberg, A. G.; Kahr, B.; Efrati, E. Twist Renormalization in Molecular Crystals Driven by Geometric Frustration. *Soft Matter* **2019**, *15* (1), 116–126. <https://doi.org/10.1039/C8SM01290C>.
- (45) Srivastava, S.; Santos, A.; Critchley, K.; Kim, K.-S.; Podsiadlo, P.; Sun, K.; Lee, J.; Xu, C.; Lilly, G. D.; Glotzer, S. C.; Kotov, N. A. Light-Controlled Self-Assembly of Semiconductor Nanoparticles into Twisted Ribbons. *Science* **2010**, *327* (5971), 1355–1359. <https://doi.org/10.1126/science.1177218>.
- (46) Mokashi-Punekar, S.; Zhou, Y.; Brooks, S. C.; Rosi, N. L. Construction of Chiral, Helical Nanoparticle Superstructures: Progress and Prospects. *Adv. Mater.* **2020**, *32* (41), 1905975.
- (47) Deng, J.; Dong, W.; Socher, R.; Li, L.-J.; Li, K.; Fei-Fei, L. Imagenet: A Large-Scale Hierarchical Image Database. In *2009 IEEE conference on computer vision and pattern recognition*; 2009; pp 248–255.
- (48) Lin, T.-Y.; Maire, M.; Belongie, S.; Hays, J.; Perona, P.; Ramanan, D.; Dollár, P.; Zitnick, C. L. Microsoft Coco: Common Objects in Context. In *European conference on computer vision*; 2014; pp 740–755.
- (49) Koch, G.; Zemel, R.; Salakhutdinov, R.; others. Siamese Neural Networks for One-Shot Image Recognition. In *ICML deep learning workshop*; 2015; Vol. 2.
- (50) Ranasinghe, T.; Orăsan, C.; Mitkov, R. Semantic Textual Similarity with Siamese Neural

- Networks. In *Proceedings of the International Conference on Recent Advances in Natural Language Processing (RANLP 2019)*; 2019; pp 1004–1011.
- (51) Jeon, M.; Park, D.; Lee, J.; Jeon, H.; Ko, M.; Kim, S.; Choi, Y.; Tan, A.-C.; Kang, J. ReSimNet: Drug Response Similarity Prediction Using Siamese Neural Networks. *Bioinformatics* **2019**, *35* (24), 5249–5256.
- (52) Wang, J.; Fang, Z.; Lang, N.; Yuan, H.; Su, M.-Y.; Baldi, P. A Multi-Resolution Approach for Spinal Metastasis Detection Using Deep Siamese Neural Networks. *Comput. Biol. Med.* **2017**, *84*, 137–146.
- (53) Wetzels, S. J.; Melko, R. G.; Scott, J.; Panju, M.; Ganesh, V. Discovering Symmetry Invariants and Conserved Quantities by Interpreting Siamese Neural Networks. *Phys. Rev. Res.* **2020**, *2* (3), 33499.
- (54) Li, M. D.; Chang, K.; Bearce, B.; Chang, C. Y.; Huang, A. J.; Campbell, J. P.; Brown, J. M.; Singh, P.; Hoebel, K. V.; Erdogmus, D.; others. Siamese Neural Networks for Continuous Disease Severity Evaluation and Change Detection in Medical Imaging. *NPJ Digit. Med.* **2020**, *3* (1), 1–9.
- (55) Chopra, S.; Hadsell, R.; LeCun, Y. Learning a Similarity Metric Discriminatively, with Application to Face Verification. In *2005 IEEE Computer Society Conference on Computer Vision and Pattern Recognition (CVPR'05)*; 2005; Vol. 1, pp 539–546.
- (56) Chechik, G.; Sharma, V.; Shalit, U.; Bengio, S. Large Scale Online Learning of Image Similarity Through Ranking. *J. Mach. Learn. Res.* **2010**, *11* (3).
- (57) Schroff, F.; Kalenichenko, D.; Philbin, J. Facenet: A Unified Embedding for Face Recognition and Clustering. In *Proceedings of the IEEE conference on computer vision and pattern recognition*; 2015; pp 815–823.
- (58) Bromley, J.; Bentz, J. W.; Bottou, L.; Guyon, I.; LeCun, Y.; Moore, C.; Säckinger, E.; Shah, R. Signature Verification Using a “Siamese” Time Delay Neural Network. *Int. J. Pattern Recognit. Artif. Intell.* **1993**, *7* (04), 669–688.
- (59) Shorten, C.; Khoshgoftaar, T. M. A Survey on Image Data Augmentation for Deep Learning. *J. Big Data* **2019**, *6* (1), 1–48.
- (60) Tan, M.; Le, Q. Efficientnet: Rethinking Model Scaling for Convolutional Neural Networks. In *International Conference on Machine Learning*; 2019; pp 6105–6114.
- (61) Hendrycks, D.; Gimpel, K. Gaussian Error Linear Units (Gelu). *arXiv Prepr.*

*arXiv1606.08415* **2016**.

- (62) Kingma, D. P.; Ba, J. Adam: A Method for Stochastic Optimization. *arXiv Prepr. arXiv1412.6980* **2014**.
- (63) Smith, L. N.; Topin, N. Super-Convergence: Very Fast Training of Neural Networks Using Large Learning Rates. In *Artificial Intelligence and Machine Learning for Multi-Domain Operations Applications*; 2019; Vol. 11006, p 1100612.
- (64) Tibshirani, R.; Hastie, T.; Narasimhan, B.; Chu, G. Diagnosis of Multiple Cancer Types by Shrunk Centroids of Gene Expression. *Proc. Natl. Acad. Sci.* **2002**, *99* (10), 6567–6572.
- (65) Hinton, G.; Roweis, S. T. Stochastic Neighbor Embedding. In *NIPS*; 2002; Vol. 15, pp 833–840.
- (66) Simonyan, K.; Vedaldi, A.; Zisserman, A. Deep inside Convolutional Networks: Visualising Image Classification Models and Saliency Maps. *arXiv Prepr. arXiv1312.6034* **2013**.
- (67) Selvaraju, R. R.; Cogswell, M.; Das, A.; Vedantam, R.; Parikh, D.; Batra, D. Grad-CAM: Visual Explanations from Deep Networks via Gradient-Based Localization. In *Proceedings of the IEEE international conference on computer vision*; 2017; pp 618–626.
- (68) Tremblay, J.; Prakash, A.; Acuna, D.; Brophy, M.; Jampani, V.; Anil, C.; To, T.; Cameracci, E.; Boochoon, S.; Birchfield, S. Training Deep Networks with Synthetic Data: Bridging the Reality Gap by Domain Randomization. In *Proceedings of the IEEE conference on computer vision and pattern recognition workshops*; 2018; pp 969–977.
- (69) Dunn, K. W.; Fu, C.; Ho, D. J.; Lee, S.; Han, S.; Salama, P.; Delp, E. J. DeepSynth: Three-Dimensional Nuclear Segmentation of Biological Images Using Neural Networks Trained with Synthetic Data. *Sci. Rep.* **2019**, *9* (1), 1–15.
- (70) Xie, W.; Noble, J. A.; Zisserman, A. Microscopy Cell Counting and Detection with Fully Convolutional Regression Networks. *Comput. methods Biomech. Biomed. Eng. Imaging & Vis.* **2018**, *6* (3), 283–292.
- (71) Courtland, R.; Honan, M.; Nordrum, A.; Reilly, M.; Rotman, D. 10 Breakthrough Technologies 2022 <https://www.technologyreview.com/2022/02/23/1045416/10-breakthrough-technologies-2022/>.
- (72) Rühle, B.; Krumrey, J. F.; Hodoroaba, V.-D. Workflow towards Automated Segmentation

of Agglomerated, Non-Spherical Particles from Electron Microscopy Images Using Artificial Neural Networks. *Sci. Rep.* **2021**, *11* (1), 1–10.

- (73) Jocher, G.; Stoken, A.; Chaurasia, A.; Borovec, J.; NanoCode012; TaoXie; Kwon, Y.; Michael, K.; Changyu, L.; Fang, J.; V, A.; Laughing; Tkianai; YxNONG; Skalski, P.; Hogan, A.; Nadar, J.; Imyhxy; Mammana, L.; AlexWang1900; Fati, C.; Montes, D.; Hajek, J.; Diaconu, L.; Minh, M. T.; Marc; Albinxavi; Fatih; Oleg; Wanghaoyang0106. YOLOv5n “Nano” models, Roboflow integration, TensorFlow export, OpenCV DNN support (v6.0) <https://github.com/ultralytics/yolov5>.  
<https://doi.org/10.5281/zenodo.5563715>.
- (74) Yan, J.; Feng, W.; Kim, J.-Y.; Lu, J.; Kumar, P.; Mu, Z.; Wu, X.; Mao, X.; Kotov, N. Self-Assembly of Chiral Nanoparticles into Semiconductor Helices with Tunable near-Infrared Optical Activity. *Chem. Mater.* **32** (1), 476–488.  
<https://doi.org/10.1021/acs.chemmater.9b04143>.
- (75) Ma, W.; Xu, L.; De Moura, A. F.; Wu, X.; Kuang, H.; Xu, C.; Kotov, N. A. Chiral Inorganic Nanostructures. *Chem. Rev.* **2017**, *117* (12).  
<https://doi.org/10.1021/acs.chemrev.6b00755>.